

DOCUMENT CONTROL DATA - R & D

(Security classification of title, body of abstract and indexing annotation must be entered when the overall report is classified)

1. ORIGINATING ACTIVITY (Corporate author) New Mexico Institute of Mining and Technology Socorro, NM	2a. REPORT SECURITY CLASSIFICATION UNCLASSIFIED
	2b. GROUP

1

3. REPORT TITLE
Some Characteristics of a Propagating Brittle Tensile Crack

4. DESCRIPTIVE NOTES (Type of report and inclusive dates)
Scientific.....Interim

5. AUTHOR(S) (First name, middle initial, last name)
Dr. Merle E. Hanson and Allan R. Sanford

6. REPORT DATE Jun 1970	7a. TOTAL NO. OF PAGES 36	7b. NO. OF REFS 13
----------------------------	------------------------------	-----------------------

8. CONTRACT OR GRANT NO. F44620-70-C-0055 ✓ 9. PROJECT NO. AO 1031 62701D	9a. ORIGINATOR'S REPORT NUMBER(S)
	9b. OTHER REPORT NO(S) (Any other numbers that may be assigned this report) AFOSR - TR - 71 - 2397

10. DISTRIBUTION STATEMENT
Approved for public release;
distribution unlimited.

11. SUPPLEMENTARY NOTES TECH, OTHER	12. SPONSORING MILITARY ACTIVITY AF Office of Scientific Research (NPG) 1400 Wilson Boulevard Arlington, VA 22209
--	--

13. ABSTRACT
A numerical technique was used to formulate the two-dimensional equations of motion for an elastic continuum. A brittle tensile crack was simulated to form and propagate in the continuum. The stress field in front of the fracture tip was found to become increasingly hydrostatic with increasing fracture velocity. A fracture criterion in terms of the values of the principal stresses near the fracture tip indicated a terminal velocity for a straight running fracture of approximately 0.39 of the dilatational wave speed. Part of the elastic energy residing initially in the continuum accumulated at the fracture tip. A quantitative fit of the elastic energy as a function of crack half-length and velocity showed that energy increases with fracture length and decreases with fracture velocity.

DDC
RECEIVED
SEP 28 1971
A

Reproduced by
NATIONAL TECHNICAL
INFORMATION SERVICE
Springfield, Va. 22151

**BEST
AVAILABLE COPY**

25 JUN 1970

AFOSR - TR - 71 - 2397

SOME CHARACTERISTICS OF A PROPAGATING
BRITTLE TENSILE CRACK



BY

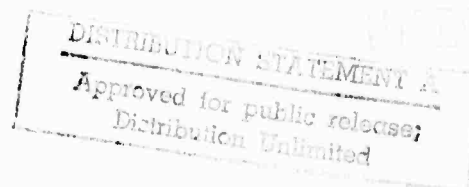
Merle E. Hanson and Allan R. Sanford

ARPA Order No.	1031 Amendment No. 4
Program Code No.	0F10
Name of Contractor	New Mexico Institute of Mining and Technology
Effective date of Contract	18 November 1969
Contract Expiration Date	17 November 1970
Amount of Contract	\$35,000.00
Contract No.	F44620-70-C -0055
Principal Investigator	Merle E. Hanson
Phone	(505) 855-5312
Project Scientist	William J. Best
Phone	(202) OX4-5457
Title of Work	Artificial Stimulation of Earthquakes

Sponsored By

ADVANCED RESEARCH PROJECTS AGENCY

ARPA Order No. 1031



S U M M A R Y
of the
SEMI-ANNUAL REPORT ON THE CONTRACT
ARTIFICIAL STIMULATION OF EARTHQUAKES
Contract No. F44620-70-C-0055

SOME CHARACTERISTICS OF A PROPAGATING BRITTLE TENSILE CRACK
June 1970

The purpose of this project is to analyze dynamic stress fields in geologic media particularly those created by fracture or other source functions. Lack of realistic analytic descriptions has led to the study of dynamic fracture in strained elastic media.

A numerical technique was used to simulate the two-dimensional dynamic characteristics of a propagating brittle tensile fracture. This study has been directed toward an understanding of dynamics fracture phenomena. By imposing the condition on the calculation that the principal stress difference ahead of the fracture tip must be greater than the stress difference at an angle to the tip, a terminal velocity for a straight funning fracture of 0.39 of the dilatational wave speed was determined. An effect of a brittle tensile fracture is the increase in the parallel principal stress just ahead of the fracture tip. Higher fracture velocities result in this parallel stress increasing faster than the perpendicular stress. In other words the stress field in front of the fracture tip was found to become increasingly hydrostatic with higher fracture velocities. A polynomial function of the strain energy increase near the fracture tip with fracture length and velocity was determined. The strain energy increases with fracture length and decreases with fracture velocity.

No equipment was developed or purchased during this report period.

SOME CHARACTERISTICS OF A PROPAGATING
BRITTLE TENSILE CRACK

Merle E. Hanson and Allan R. Sanford

ABSTRACT

A numerical technique was used to formulate the two-dimensional equations of motion for an elastic continuum. A brittle tensile crack was simulated to form and propagate in the continuum. The stress field in front of the fracture tip was found to become increasingly hydrostatic with increasing fracture velocity. A fracture criterion in terms of the values of the principal stresses near the fracture tip indicated a terminal velocity for a straight running fracture of approximately 0.39 of the dilatational wave speed. Part of the elastic energy residing initially in the continuum accumulated at the fracture tip. A quantitative fit of the elastic energy as a function of crack half-length and velocity showed that energy increases with fracture length and decreases with fracture velocity.

INTRODUCTION

This paper discusses some of the dynamic characteristics of a bilateral brittle tensile fracture in an elastic continuum. The tensile crack was numerically simulated to form and propagate in an elastic media having two-dimensional plane strain characteristics. A uniform uniaxial tensile stress field was imposed on the elastic continuum for all t . The technique of calculation was to use a two-dimensional Lagrangian finite difference formulation of the elastic equations of motion. In this study, several fracture velocities were simulated. In addition, a failure criteria was applied that resulted in a calculated terminal velocity similar to that given by Dulaney and Brace (1960) and Wells and Post (1957).

The strain energy in the elastic medium in the vicinity of the fracture was affected by the propagating fracture. The energy was (1) converted to kinetic energy, (2) taken up by the creation of the fracture surfaces, and (3) accumulated at the fracture tip. A function relating the fracture velocity, energy at the fracture tip, and fracture length was obtained. Energy increases with an increase in fracture length and a decrease in fracture velocity.

Other investigators have studied the dynamic behavior of a brittle tensile crack. For example, Yoffe (1951) analyzed a constant length fracture moving with constant velocity through a brittle elastic material. Her solution showed that for large fracture velocities the stress on a radius about the crack tip was maximum at some angle to the fracture axis. Thus, at some critical fracture velocity the crack would either branch or curve. However, the solution is physically unappealing because the length of a natural tensile fracture is not constant. Craggs (1960) analyzed a two-dimensional brittle fracture extending unilaterally in an infinite elastic medium. He concluded that the force required to maintain a steady rate of extension of the crack decreases as the crack velocity increases. Baker (1962) analyzed the case for a semi-infinite crack extending at constant velocity in a stretched elastic body. Baker contends that the stress field at the fracture tip is independent of fracture length.

FORMULATION OF THE PROBLEM
AND
NUMERICAL TECHNIQUE OF SOLUTION

The boundary conditions and fracture simulation were similar to those described by Hanson and Sanford (1970). Fracture velocities were specified with the crack velocity starting and remaining at a constant value until the calculation was terminated. The fracture velocities specified in the calculations were $0.1C_1$, $0.2C_1$, $0.3C_1$, $0.39C_1$, $.45C_1$, and $.5C_1$ where C_1 is the dilatational wave speed in plane strain.

The calculational grid size was chosen so that reflections from boundaries would not reach the areas of interest in the grid. The initial stress field in the elastic media was uniaxial tension of magnitude 10^9 dynes/cm². Because of the symmetry of a bilateral tensile fracture, the problem could be solved by carrying out calculations in one quadrant only. In the calculation, the energy required to create the fracture surface was taken as approximately 5×10^6 ergs/cm² which is in agreement with the values given by Dulaney and Brace (1960).

The operation of the numerical Lagrangian two-dimensional computer code and the formation of cracks was identical as described by Hanson and Sanford (1970). A complete discussion of the difference forms used is given in Petschek and Hanson (1968). A tensor damping form was included in these calculations to reduce the numerically

created high frequency oscillations resulting from the crack opening in a discretized mass network. The damping tensor is obtained from the time rate of change of the strain tensor.

The forms of damping used include both linear damping and quadratic damping. The quadratic damping is defined by

$$\begin{aligned} q_{xx} &= K_1 (\dot{\epsilon}_{xx})^2, \\ q_{yy} &= K_1 (\dot{\epsilon}_{yy})^2, \\ \text{and } q_{xy} &= K_1 (\dot{\epsilon}_{xy})^2. \end{aligned} \quad (1)$$

The linear form of the damping used is

$$\begin{aligned} q_{xx} &= K_2 \dot{\epsilon}_{xx}, \\ q_{yy} &= K_2 \dot{\epsilon}_{yy}, \\ \text{and } q_{xy} &= K_2 \dot{\epsilon}_{xy}, \end{aligned} \quad (2)$$

where

$$\begin{aligned} K_1 &= \frac{C_q^2 \rho_0 \Lambda^{n+1/2}}{V^{n+1/2}} \\ K_2 &= \frac{a C_L \rho_0 \sqrt{\Lambda^{n+1/2}}}{V^{n+1/2}}, \end{aligned} \quad (3)$$

C_q, C_L are constants,
 a is the P-wave speed,
 ρ_0 is the initial density,
 ϵ_{ii} is the strain and
 $\Lambda^{n+1/2}, V^{n+1/2}$

are the area and volume of the Lagrangian zone defined as the average between the n and $n + 1$ time steps. Application of the damping is accomplished by simply adding similar terms of the damping and stress tensors before application to the momentum equations. In addition energy conservation is assured in the calculation if the sum is also applied in the energy equation.

The properties of these damping forms has been worked out by Petschek (1970). If the effect of heating is ignored, a one-dimensional form of the elastic wave equation, with linear and quadratic damping is

$$\frac{\partial^2 u}{\partial t^2} = \frac{E}{\rho} \frac{\partial^2 u}{\partial y^2} + C'_L \frac{\partial^2}{\partial y^2} \frac{\partial u}{\partial t} + C'_q \frac{\partial}{\partial y} \left(\frac{\partial}{\partial y} \frac{\partial u}{\partial t} \right)^2 \quad (4)$$

where E is Young's modulus and ρ is density, and C'_L and C'_q are the coefficients of the linear and quadratic damping. Multiplication of this equation by $\partial u / \partial t$, and integration by parts over the length of the rod with the boundary conditions $\partial u / \partial y = 0$ leads to

$$\frac{\partial}{\partial t} \int \left[\frac{1}{2} \left(\frac{\partial u}{\partial t} \right)^2 + \frac{1}{2} \frac{E}{\rho} \left(\frac{\partial u}{\partial y} \right)^2 \right] dy = -C'_L \int \left(\frac{\partial u}{\partial y \partial t} \right)^2 dy - C'_q \int \left(\frac{\partial^2 u}{\partial y \partial t} \right)^3 dy. \quad (5)$$

The left side of the preceding equation is the time derivative of the energy of the system. If the amplitude of the oscillation is A , the frequency ω , and the length L , then the integral is $A^2 \omega^2 L$ except for a constant. The term

$\partial^2 u / \partial y \partial t$ is proportional to $\Lambda \omega^2 / V$, where V is the wave speed.
Hence the equation can be written as

$$\frac{\partial}{\partial t} A^2 \omega^2 L = -C_L'' A^2 \omega^4 L / V^2 - C_q'' \Lambda^3 \omega^6 L / V^3 \quad (6)$$

where C_L'' and C_q'' are new constants. The equation is finally

$$\frac{\partial A}{\partial t} = \frac{-C_L'' \omega^2}{2V^2} A - \frac{C_q'' \omega^4 \Lambda^2}{2V^3} \quad (7)$$

If the second term on the right is ignored, the linear damping gives exponential decay. The quadratic damping gives

$$\frac{1}{A} = \frac{1}{\Lambda_0} + C_q''' t, \quad (8)$$

or $A \sim 1/t$ an effective damping proportional to the amplitude. In addition the damping increases rapidly with frequency.

In the above discussion, the oscillations are assumed small. The damping is used primarily to reduce the numerically created oscillations resulting from the technique used to simulate the moving fracture.

CHARACTERISTICS OF THE STRESS FIELD

The initial uniaxial stress field of the medium is modified by the introduction of a moving fracture particularly in the vicinity of the crack tip. An effect of a dynamically propagating tensile crack is the creation just ahead of the fracture tip of tensile stress parallel to the fracture axis. As the fracture length increases this tensile stress as well as that perpendicular to the fracture axis increases. However, with increasing fracture velocity, the parallel stress increases faster than the perpendicular stress. In other words, there is a tendency toward a hydrostatic condition. For example, Figure 1 shows that the ratio σ_1/σ_2 increases slower for a fracture velocity of $0.2C_1$ than for higher fracture velocities (σ_1 is the principal stress parallel to the crack and σ_2 is the principal perpendicular stress). This ratio is sensitive to damping in the calculation.

For this analysis the scaling was chosen so that the Lagrangian zone was one centimeter square. Because the computational technique implies that the stresses are an average over the Lagrangian zone, interpretations of the stresses closer than a half zone to the singularity at the crack tip are not possible. Therefore, the stresses can only be compared a half zone ahead of the crack tip.

Possible confirmation of a dilated region in front of the crack tip comes from experiments of Wells and Post (1957). They experienced difficulty with a region near the tip of the crack in photoelastic experiments. For a tensile crack propagating in the photoelastic material, they reported that a distortion resulting in a surface dimple in the region near the tip of the crack caused extinction of light in this region. The dimpling effect is the result of the buildup of the parallel stress tending to a more hydrostatic field in the region.

Figure 2 is a plot of the principal axis of stress (tensile) over the region about the right crack tip. If branch fractures are to form they should be oriented perpendicular to these principal stresses. A branch fracture which originates in the region ahead of the fracture tip will tend toward the original fracture axis. A branch fracture which originates just behind the fracture tip will tend to diverge from the original fracture axis. Figure 2 is in agreement with the experimental results of Manogg (1966).

Figures 3 and 4 depict the rotation of the principal axes of stress as a moving fracture tip passes beneath the point. Again Manogg (1966) shows comparable results from an experiment. Examination of these figures shows that the amount and rate of rotation of the principal axis

increases with fracture length. In addition, the rotation rate and magnitude increase with fracture velocity. In the times considered on these plots, the principal axis angle is negative at the start. The negative angle results from the flow of material toward the fracture tip. The rotation indicates the changing shear stress in the region.

Figure 5 is a contour plot of $2\tau = \sigma_2 - \sigma_1$ where σ_2 and σ_1 are the principal stresses and τ is the maximum shear stress. Notice that the principal lobe is at an angle greater than 45° to the fracture axis. On the other hand, there is a minimum lobe directly in front of the fracture tip. The minimum lobe indicates a decrease in distortion due to increasing hydrostatic tension in the region. The distortional pattern increases with fracture length. The relaxation zone behind the fracture tip expands at P-wave velocity. Contours of constant dilatation are shown on Figure 6. The maximum is directly in front of the fracture tip and the minimum occurs at the crack face in the expansion region behind the tip.

TERMINAL VELOCITY OF A STRAIGHT RUNNING FRACTURE

The terminal velocity of a straight running fracture is defined as the maximum velocity at which a crack will expand without branching. If the terminal velocity of a straight running fracture is a function of the dynamic stress field at the tip of the fracture, then it should be possible to establish a criterion for a straight running fracture in terms of the principal values of stresses at the fracture tip. Let the principal stress difference $1/2$ zone ahead of the crack tip be defined as $(\sigma_2 - \sigma_1)_a$ and 1 zone this point $(\sigma_2 - \sigma_1)_b$. A measure of the relative elongation between the principal axis is $(\epsilon_2 - \epsilon_1)$. For a Hookean material, the strain difference differs from the stress difference by only a constant, $(\sigma_2 - \sigma_1) = 2\mu(\epsilon_2 - \epsilon_1)$, and therefore the strain ellipse has the same shape as the stress ellipse.

Figure 7 shows the ratio of the stress difference at b to the stress difference at a , $(\sigma_2 - \sigma_1)_b / (\sigma_2 - \sigma_1)_a$, for the fracture velocities $0.2C_1$, $0.3C_1$, $0.39C_1$, $0.45C_1$, and $0.5C_1$ as a function of crack half length. For the fracture velocities less than or equal to $0.39C_1$, the ratio is less than one. However, at the velocity $0.45C_1$, the ratio exceeds this value after the crack has run a short distance. Hence the eccentricity of the strain ellipse becomes greater at b than a for velocities larger

than $0.39C_1$. The terminal velocity $0.39C_1$ is obtained by applying the criteria that the stress difference had to be greater at a than it was at b. In equation form the criteria chosen was

$$(\sigma_2 - \sigma_1)_a > G (\sigma_2 - \sigma_1)_b$$

and

$$(\sigma_2 - \sigma_1)_a > HP$$

(9)

where H is a constant, taken at 1.2 and P is the magnitude of the initial uniaxial stress. The resulting calculation predicts a terminal velocity of $0.39C_1$, as a maximum. Lower velocities, down to about $0.37C_1$, can be predicted by using other time steps for the calculation. The terminal velocities predicted bracket the velocity of $0.38C_1$ given in Wells and Post (1957). Variation of the parameter G over a range of 1.1 to 1.3 did not effect the terminal velocity.

STRAIN ENERGIES

Examination of Figures 8, 9, and 10 shows that strain energy at the fracture tip increases in a non-linear manner with fracture length. The strain energy depicted on these plots is the strain energy in excess of the initial strain energy. In equation form, the energy discussed is

$$E'_\alpha = E_\alpha^{(n)} - E_\alpha^{(o)}, \quad (10)$$

where $E_\alpha^{(n)}$ can be the dilatational, distortional or the total strain energy at time t and $E_\alpha^{(o)}$ is the initial value of the elastic energies. The elastic energies are integrated over a region where their value is greater than the initial value at that time. The integration is performed numerically in a region near the crack tip. Hence the magnitude of the energy shown on the plots is energy in excess of the initial over the region determined to have excess strain energy.

The integrations were performed only over the regions where the elastic energies were larger than their initial values because these are the areas which can affect the propagating fracture. For example, if the total elastic energy decreased, the fracture could be expected to slow up or stop. On the other hand, excessive concentration of energy off the fracture axis could be expected to result in a branch or change in direction of the fracture.

Because only the energies larger than the initial energies were included in the integration, the sum of the dilatational and distortional parts does not necessarily have to equal the total elastic energy.

Figures 11, 12, and 13 show an example of the regions which have dilatational, distortional or total strain energies in excess of the initial values. Figure 11 depicts the region where the dilatational strain energy increases ahead of the crack tip. Except for a narrow band directly in front of the crack tip, both the distortional and total strain energies decrease in this area. The plots shown are for a fracture velocity of $0.3C_1$. The velocity has been non-dimensionalized for these plots by forming the ratio $\lambda = V_f/C_1$, where V_f is the fracture velocity and C_1 is the compressional wave velocity. A similarity exists in the shape of the regions where the distortional and total strain energies are larger than the initial elastic energies near the crack tip; however, the distortional region has a larger extent with a narrower band at the tip.

The elastic energies near the crack tip increase with fracture length and decrease with fracture velocity. However, the decrease in elastic energy with fracture velocity to the velocity $\lambda = .39$ does not result in a net decrease of elastic energy with crack length. Increase in fracture velocity results in the dilatational energy decreasing

slower than the total or distortional energy. In addition to the increase in the magnitude of total strain energy in the near vicinity to the tip with crack length, the size of the regions having strain energies greater than the initial value increase with crack length.

A functional form to describe the change in energy was obtained by performing a two dimensional fit of energy as a function of crack half length in centimeters and non-dimensional velocity λ . The functions presented are not unique and are shown to provide quantitative relationships. The equations are for perfectly elastic materials with energy dissipation resulting primarily from the creation of the fracture surfaces. The fit was performed for half crack lengths of 2 to 12 centimeters and non-dimensional velocities, λ , of 0.1 to 0.39. Cubic polynomials were chosen with differences between the fit and the calculated values of not more than 15%. The units on the energies are megabars-cm³. The cubic terms are small on the dilatational energy fit but are more significant on the total and distortional fits. The polynomial equations are

$$E'_{\alpha} = \beta_1 + \beta_2 x + \beta_3 \lambda + \beta_4 x^2 + \beta_5 x\lambda + \beta_6 \lambda^2 + \beta_7 x^3 + \beta_8 x^2\lambda + \beta_9 x\lambda^2 + \beta_{10} \lambda^3 \quad (11)$$

where the energies E'_{α} are defined in equation (10), and the parameters β are given in Table 1.

Examination of Figure 10 shows that a fracture can decrease the rate of energy accumulation at the tip by accelerating to a higher velocity. However, higher velocities cause the stress field to become more hydrostatic.

The brittle dynamic fracture of these calculations differs from a stable Griffith type fracture in that energy in excess of that required to form the fracture surface accumulates near the fracture tip. The physical effect of this excess energy may be to increase fracture roughness. An increase of fracture roughness with fracture velocity has been reported by Cotterell (1965 and 1968), Craggs (1960) and Biemawski (1968). In addition, if branching is to occur, then excess energy must be available.

CONCLUSIONS

The simulation showed that a tensile stress parallel to the fracture axis is created in front of the moving crack tip. Because this tensile stress increases with crack length and/or velocity, the stress at the tip tends to become more hydrostatic as crack length and/or velocity is increased.

A terminal velocity for a straight running fracture of $0.39C_1$ was obtained from the calculation. The fracture criterion used was that the principal stress difference be greater in front of the crack tip than at an angle to the fracture axis.

The elastic energy at the fracture tip was found to increase with increase in fracture length or decrease in fracture velocity. The result that the energy and hence the crack extension force continually increase with crack length is borne out by Cotterell (1964). The region occupied by a dilatational energy in excess of the initial value was a lobe directly in front of the propagating fracture tip. The lobes of highest distortional stress were at an angle of greater than 45° to the projected axis of the fracture. The high distortional stress lobes extend forward from the fracture tip. A lobe having a distortional stress less than the initial value extends in front of the fracture tip.

ACKNOWLEDGEMENTS

The authors wish to express their appreciation to A. G. Petschek, for his many helpful suggestions. Gary Mosley and Thomas Schellhase assisted in developing computer plot routines. This research was supported by the Advanced Research Projects Agency of the Department of Defense and was monitored by the Air Force Office of Scientific Research under Contract Number F44620-70-C-0055.

REFERENCES

Baker, B. R., 1962 Dynamic stresses created by a moving crack. J. Appl. Mech., 29, 449-458.

Bieniawski, Z. T., 1968. Fracture dynamics of rock, Int. J. Frac. Mech., 4, 415-430.

Cotterell, B., 1964. On the nature of moving cracks, J. Appl. Mech., 31, Series E, 12-16.

Cotterell, B., 1965. Velocity effects in fracture propagation, Appl. Mat. Res., 4, 227-232.

Cotterell, B., 1968. Fracture propagation in organic gasses, Int. J. Frac. Mech., 4, 209-217.

Craggs, J. W., 1960. On the propagation of a crack in an elastic-brittle material, J. Mech. Phys. Solids, 8, 66-75.

Dulaney, E. N. and W. F. Brace, 1960. Velocity behavior of a growing crack, J. Appl. Phys., 31, 2233-2236.

Hanson, M.E. and A. R. Sanford, 1970. A two-dimensional source function for a dynamic brittle bilateral tensile crack, Bull. Seis. Soc. of America, to be published.

Manogg, P., 1966. Investigation of the rupture of a plexiglas plate by means of an optical method involving high-speed filming of the shadows originating around holes drilled in the plate, Int. J. Frac. Mech., 2, 604-613.

Petschek, A. G. and M. E. Hanson, 1968. Difference equations for two-dimensional elastic flow, J. Comp. Phys., 3, 307-321.

Petschek, A. G., 1970. Personal communication.

Wells, A. A. and D. Post, 1957. The dynamic stress distribution surrounding a running crack--a photoelastic analysis, Spring Meeting of the Society for Experimental Stress Analysis, Boston, Mass.

Yoffe, E. H., 1951. The moving griffith crack, Phil. Mag., 42, Series 7, 739-750.

FIGURE CAPTIONS

Figure 1

The ratio of the principal stresses $1/2$ zone ahead of the fracture tip as a function of crack half-length in centimeters for several fracture velocities.

Figure 2

Orientations of the maximum principle axis of stress for part of the upper right hand quadrant. The fracture extent is from $Y = 0, X = 0$ to $X = 11$ centimeters with the fracture tip shown by the arrow. The orientations are not shown on the fracture axis but are vertical. Fracture velocity was $0.3C_1$.

Figure 3

Rotation of the principal axis of stress as the fracture tip passes 1 zone beneath the point for crack half-lengths of 4, 7, and 10 centimeters. The reference time is in microseconds with the zero time chosen so that the point observed relative to the crack tip is identical for the three cases. Fracture velocity is $0.3C_1$.

Figure 4

Comparison of the rotation of principal axis for four fracture velocities. Crack half-length was 5 centimeters. The reference time is in microseconds with the zero time chosen so that the point observed relative to the crack tip is identical for the cases.

Figure 5

Contour plot of the maximum principal stress difference. Fracture velocity was $0.3C_1$ and fracture half-length was 5 centimeters. X and Y coordinates are in centimeters. The minimum lobe is directly in front of the fracture tip and the

FIGURE CAPTIONS, Continued

-20-

Figure 5, Continued

maximum is at about 60° to the fracture tip. Increasing contour numbers indicate increasing stress difference.

Figure 6

Contour plot of the dilatation. The fracture half-length was 5 centimeters and the fracture velocity was $0.3C_1$. The maximum lobe is in front of the fracture tip. Increasing contour numbers indicate increasing dilatation.

Figure 7

The ratio of the principal stress difference $1/2$ zone ahead and one zone above the fracture tip to the principal stress difference $1/2$ zone ahead of the fracture tip as a function of fracture half-lengths in centimeters for several fracture velocities. Note the ratio becomes greater than one for the velocity $0.45C_1$ and higher velocities.

Figure 8

The surface of E' Dilatational as a function of fracture half length in centimeters and non-dimensional velocity $\lambda = V_f/C_1$.

Figure 9

The surface of E' Distortional as a function of fracture half length in centimeters and non-dimensional velocity, $\lambda = V_f/C_1$.

Figure 10

The surface of E' Total as a function of fracture half length in centimeters and non-dimensional velocity, $\lambda = V_f/C_1$.

Figure 11

An example of the integration domain for $E'_{\text{Dilatational}}$ for a fracture half-length of 5 centimeters and a fracture velocity of $0.3C_1$. Both coordinates X and Y are in centimeters. The half fracture extends from $X = 0, Y = 0$ to a point above arrow depicting the fracture tip and is shown by the solid line. The gradient of the function decreases to the right.

Figure 12

An example of the integration domain for $E'_{\text{Distortional}}$ for a fracture half length of 5 centimeters and a fracture velocity of $0.3C_1$. Both coordinates X and Y are in centimeters. The half fracture extends from $X = 0, Y = 0$ to a point above the arrow depicting the tip and is shown by the solid line. The function decreases away from the tip and is small to the right.

Figure 13

An example of the integration domain for E'_{Total} for a fracture half length of 5 centimeters and a fracture velocity of $0.3C_1$. Both coordinates X and Y are in centimeters. The half fracture extends from $X = 0, Y = 0$ to a point above the arrow depicting the tip and is shown by the solid line. The gradient of the function decreases away from the crack tip.

TABLE 1

PARAMETERS	E' DILATATIONAL	E' DISTORTIONAL	E' TOTAL
β_1	$-.12868 \times 10^{-4}$	$-.23871 \times 10^{-4}$	$-.34752 \times 10^{-4}$
β_2	$.22578 \times 10^{-4}$	$.70699 \times 10^{-4}$	$.83393 \times 10^{-4}$
β_3	$.25982 \times 10^{-4}$	$-.13256 \times 10^{-3}$	$-.57486 \times 10^{-4}$
β_4	$.29405 \times 10^{-5}$	$.40032 \times 10^{-5}$	$.86935 \times 10^{-5}$
β_5	$-.14130 \times 10^{-3}$	$-.32245 \times 10^{-3}$	$-.50537 \times 10^{-3}$
β_6	$.29591 \times 10^{-3}$	$.11046 \times 10^{-2}$	$.14547 \times 10^{-2}$
β_7	$-.77827 \times 10^{-8}$	$-.22248 \times 10^{-6}$	$-.17051 \times 10^{-6}$
β_8	$-.63251 \times 10^{-5}$	$.38887 \times 10^{-5}$	$-.11191 \times 10^{-4}$
β_9	$.22011 \times 10^{-3}$	$.28028 \times 10^{-3}$	$.67338 \times 10^{-3}$
β_{10}	$-.71616 \times 10^{-3}$	$-.13615 \times 10^{-2}$	$-.25326 \times 10^{-2}$

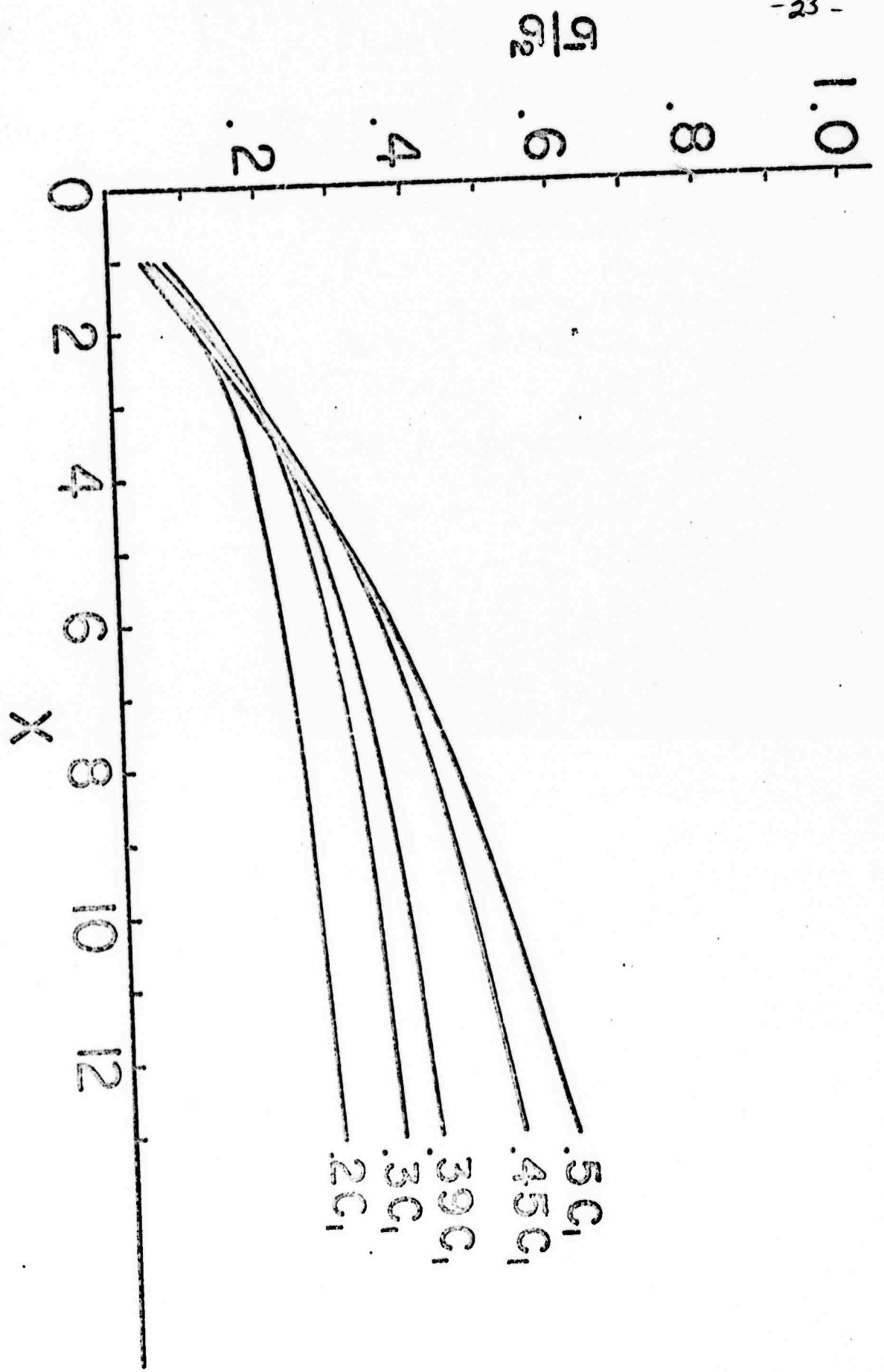
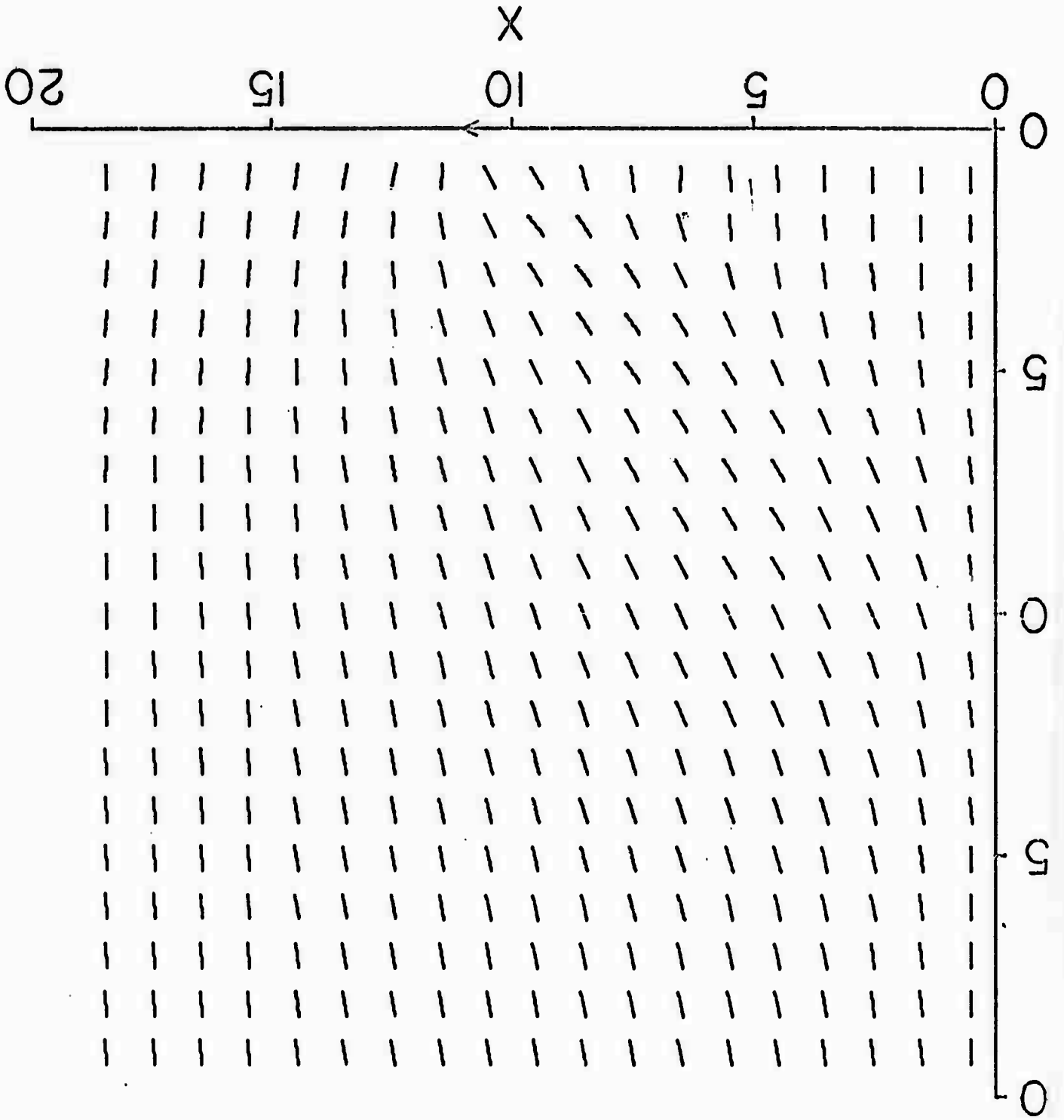
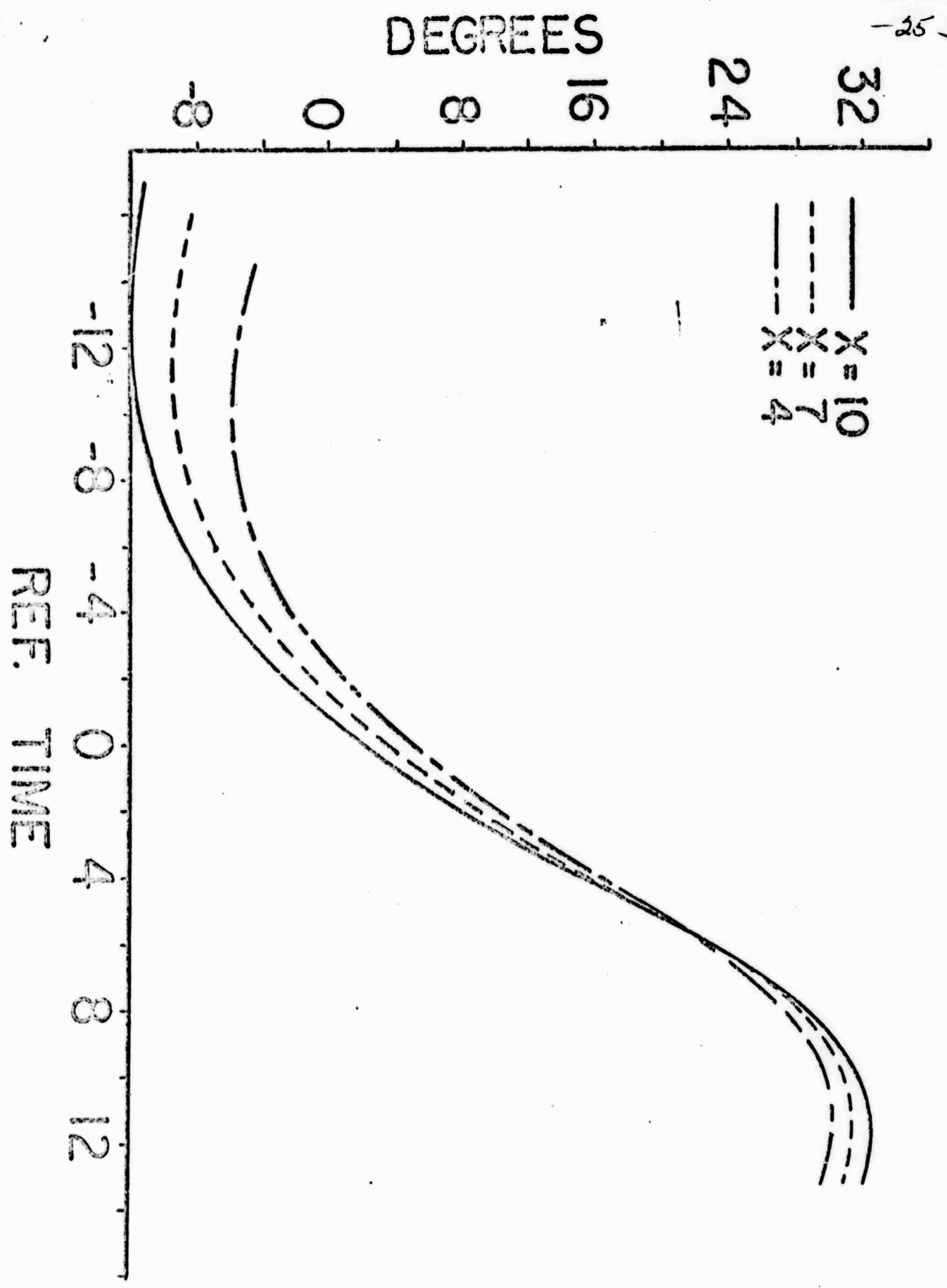
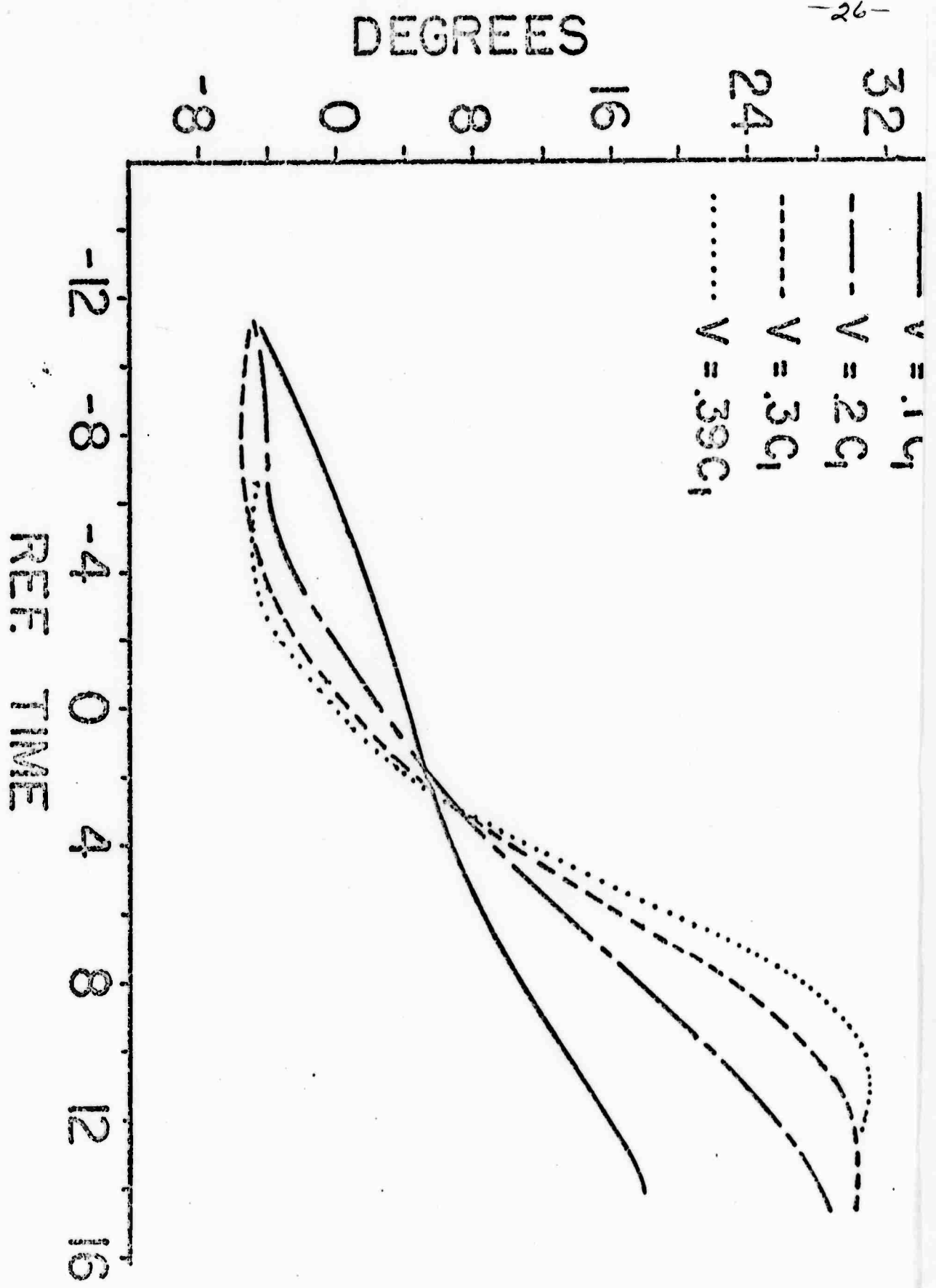


Fig. 1

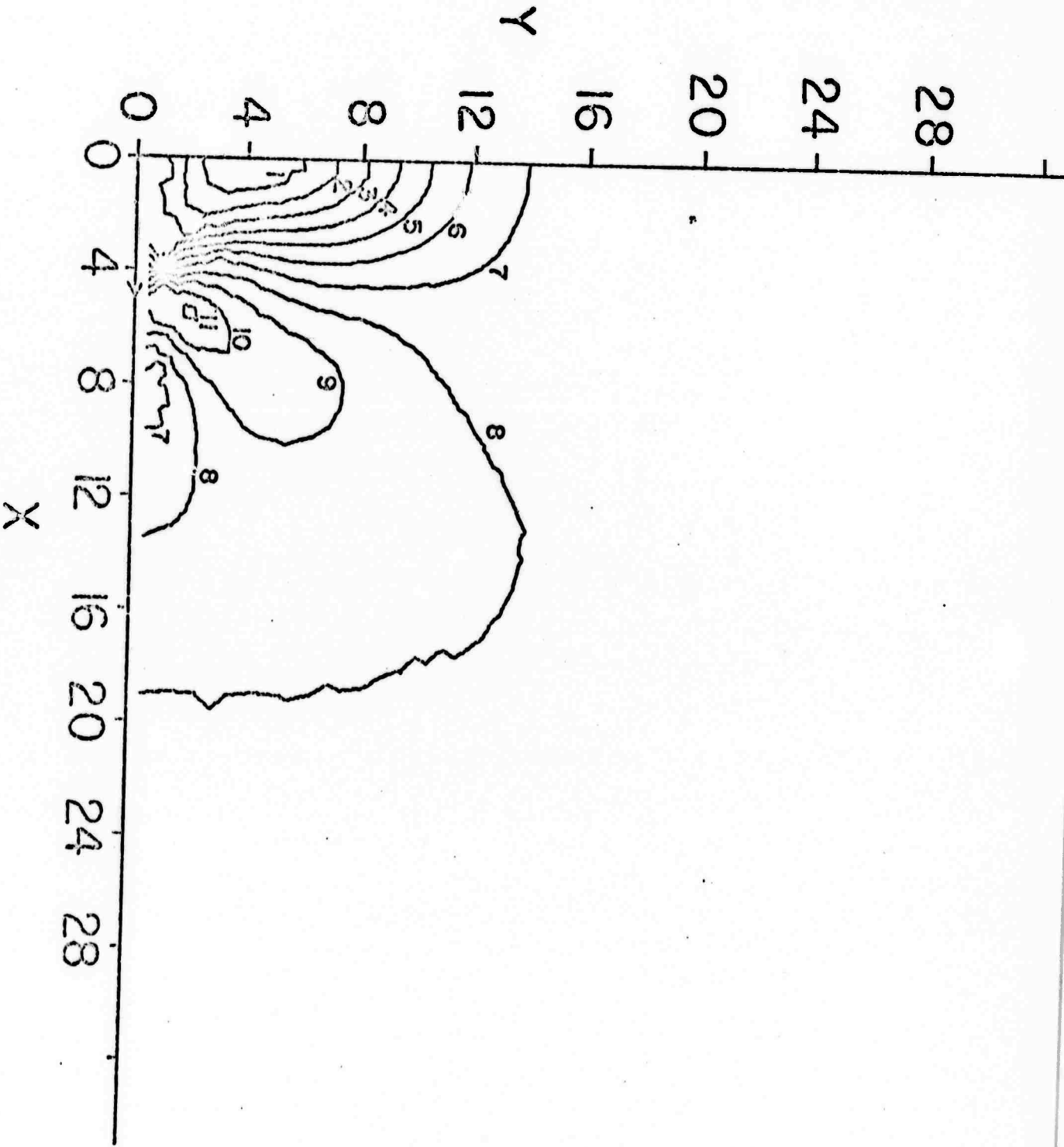


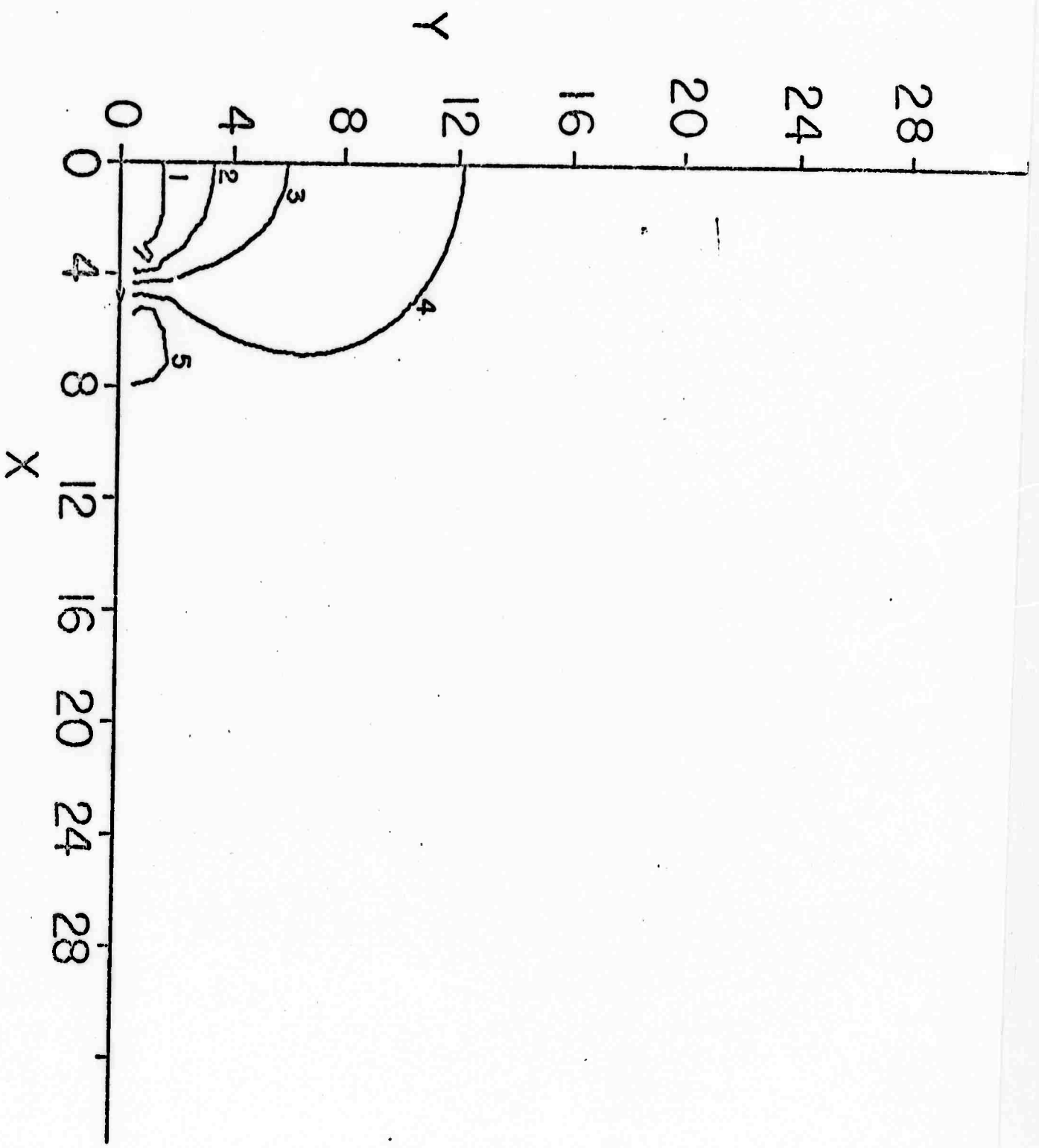


is

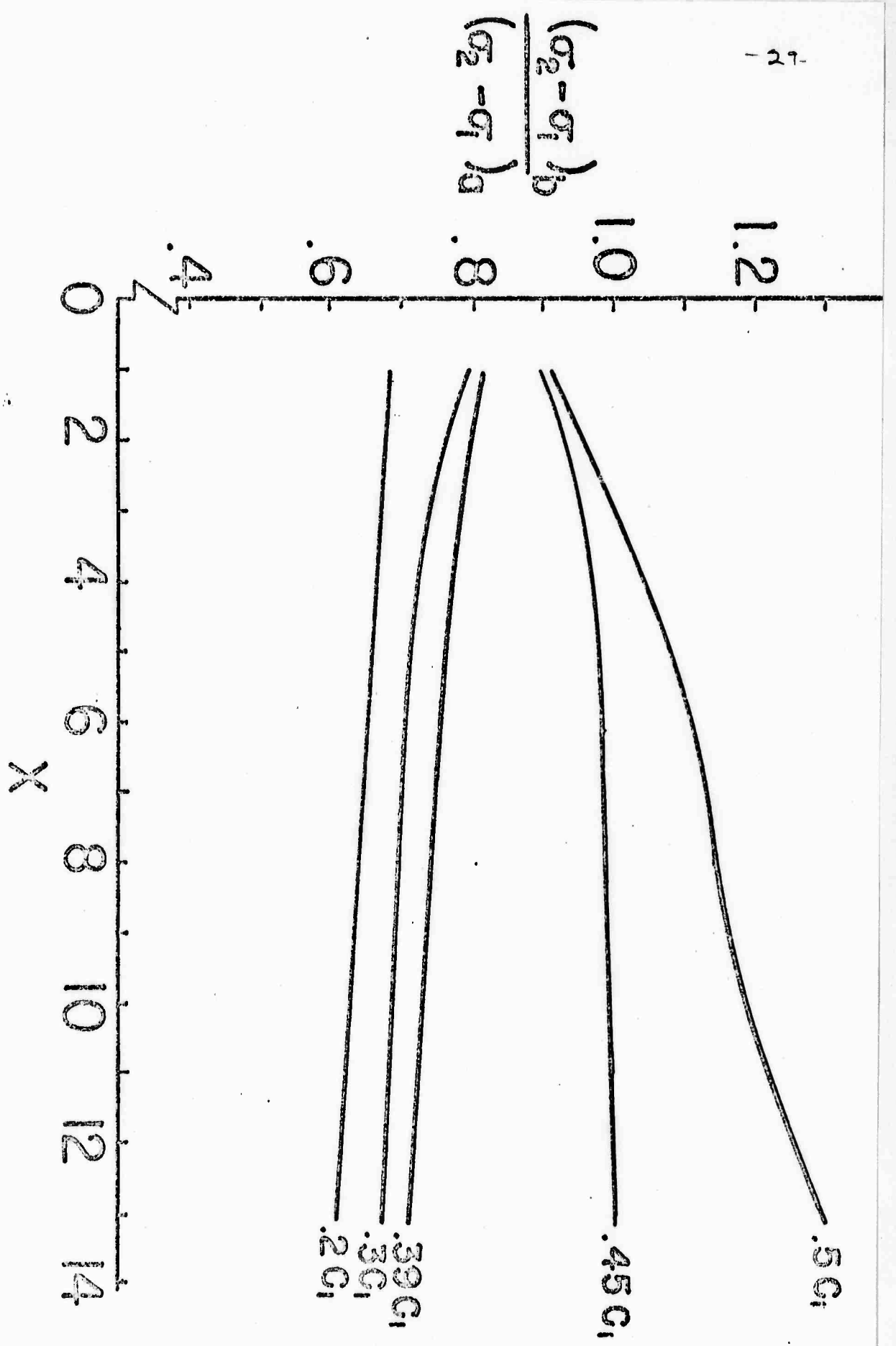


16.5

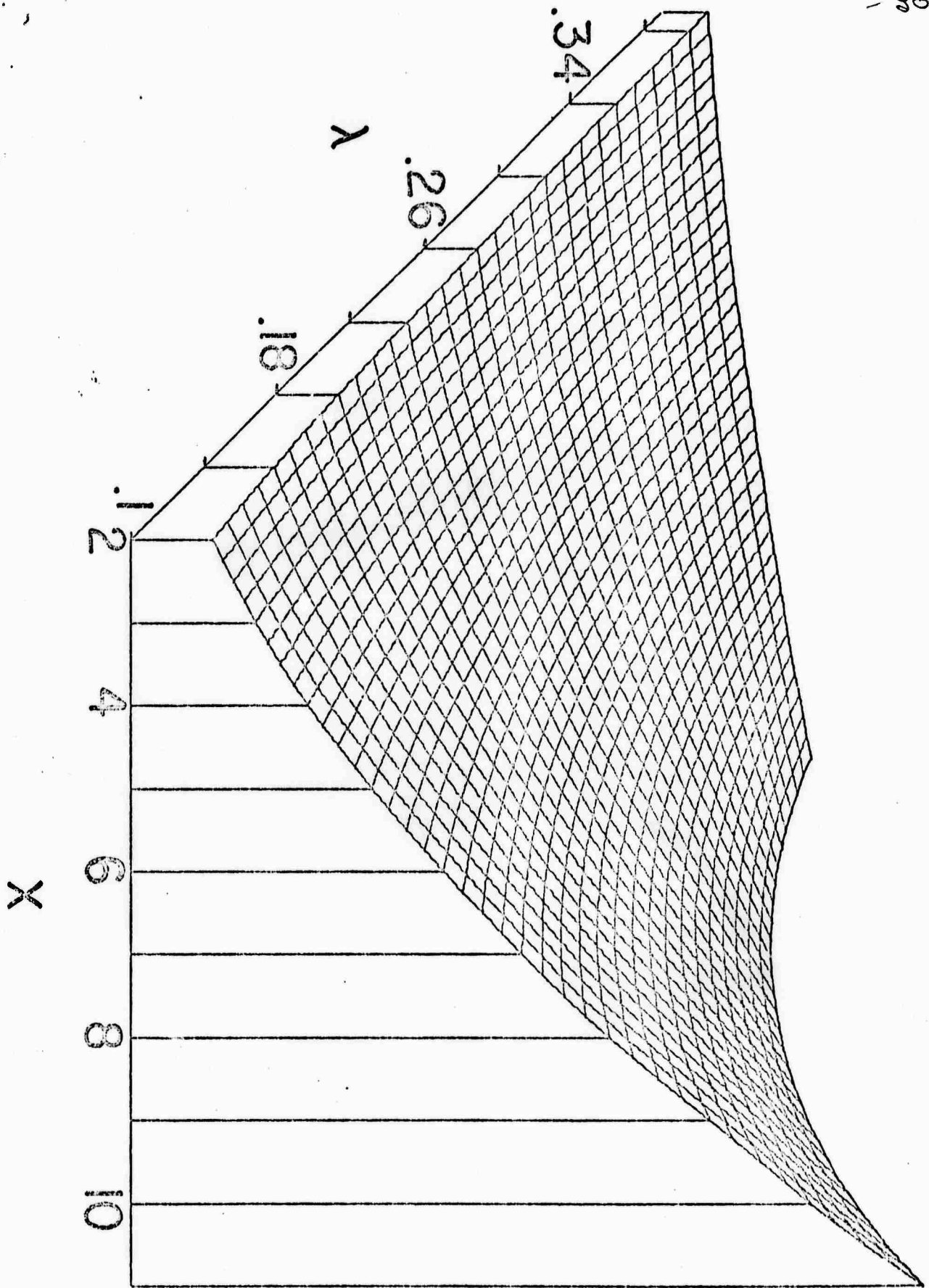


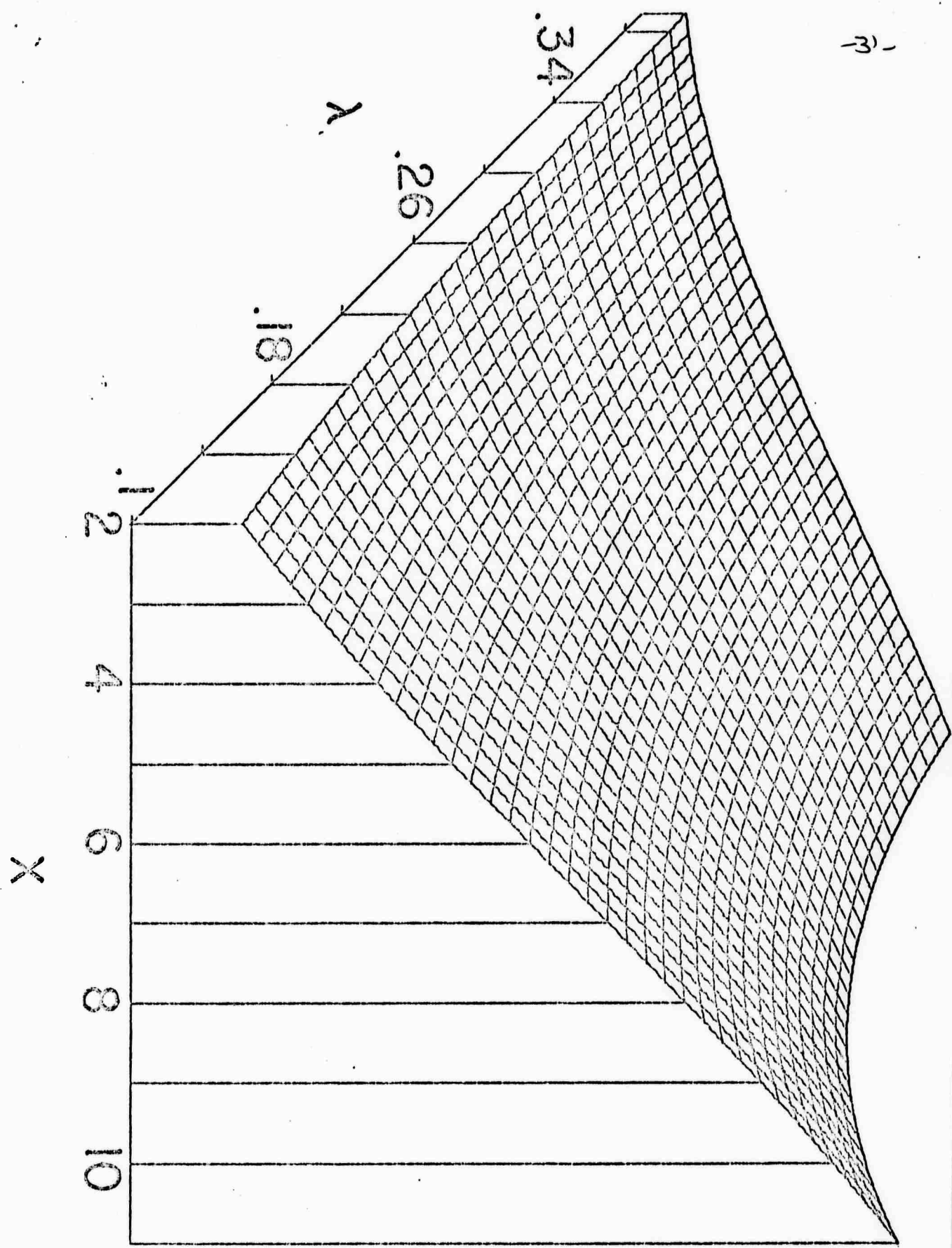


4.6

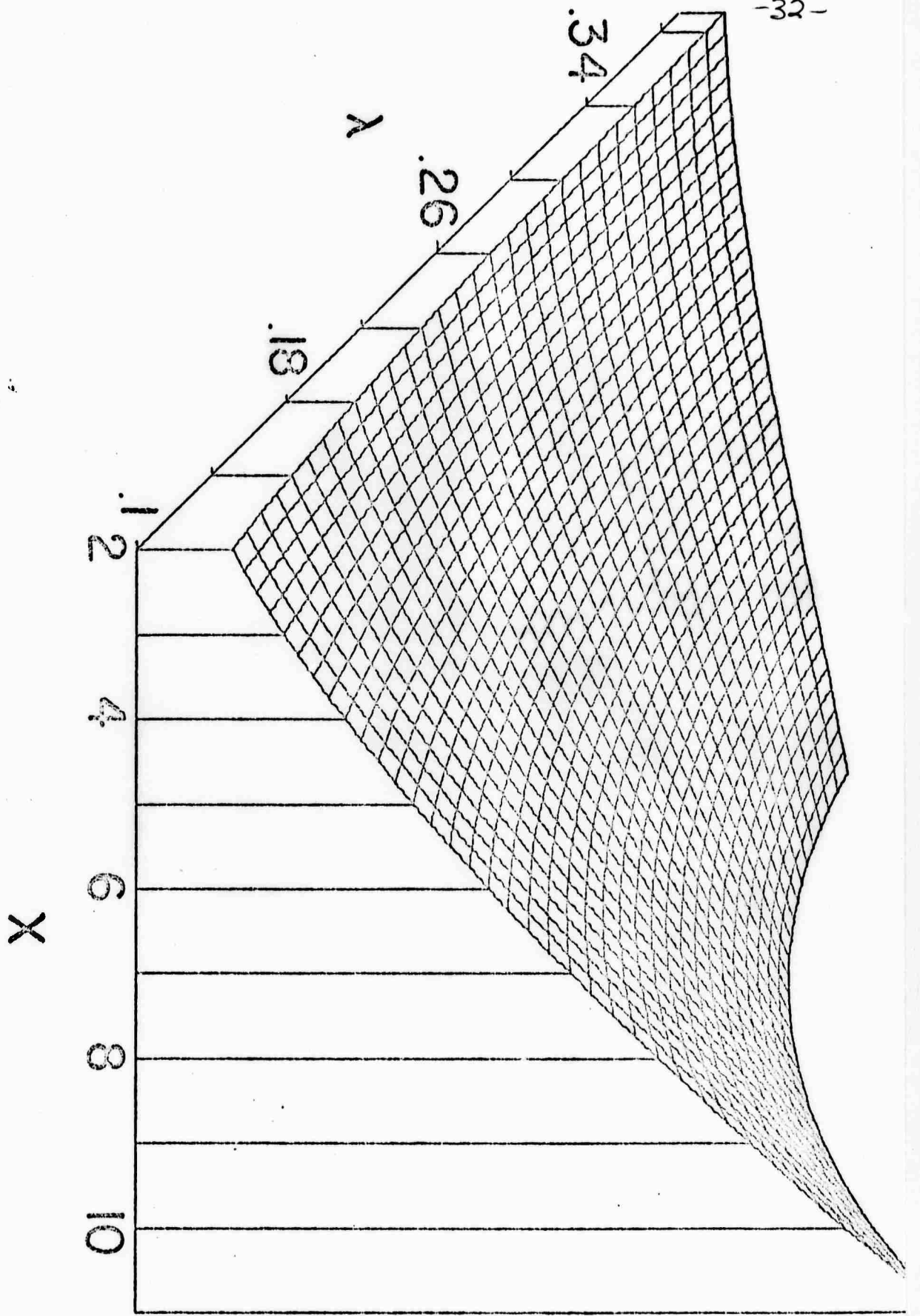


G. 7



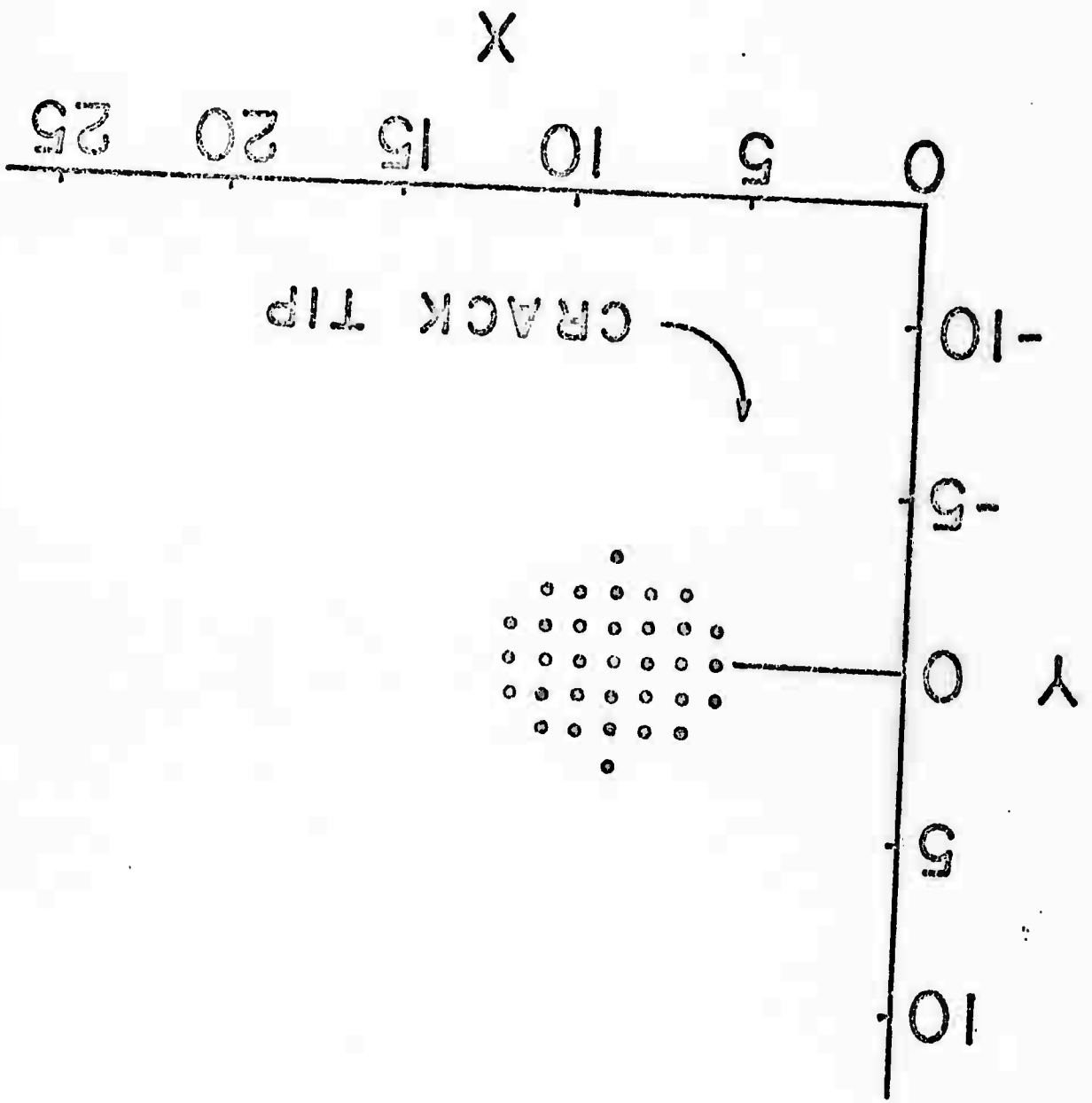


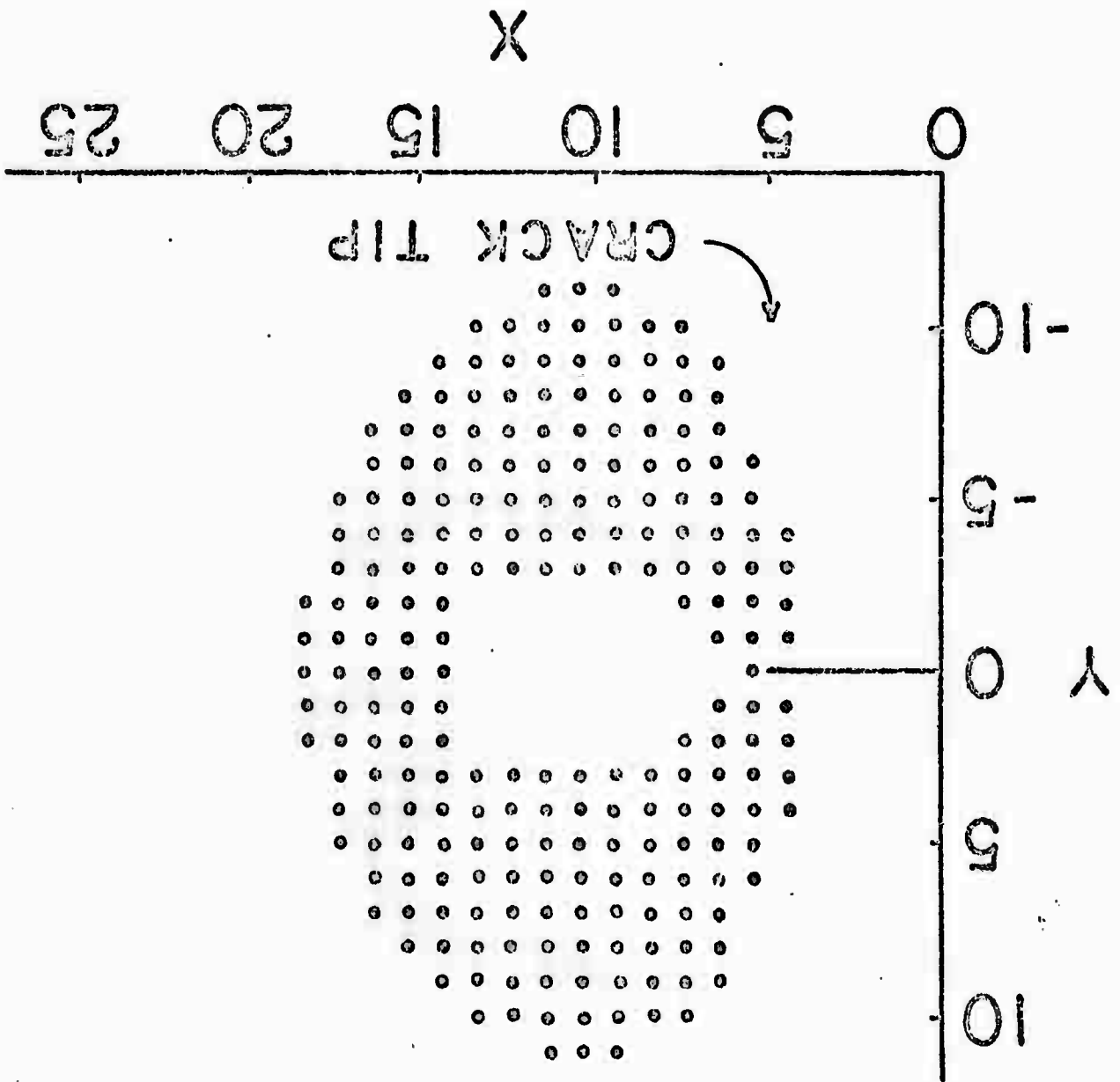
5.9



16.10

4





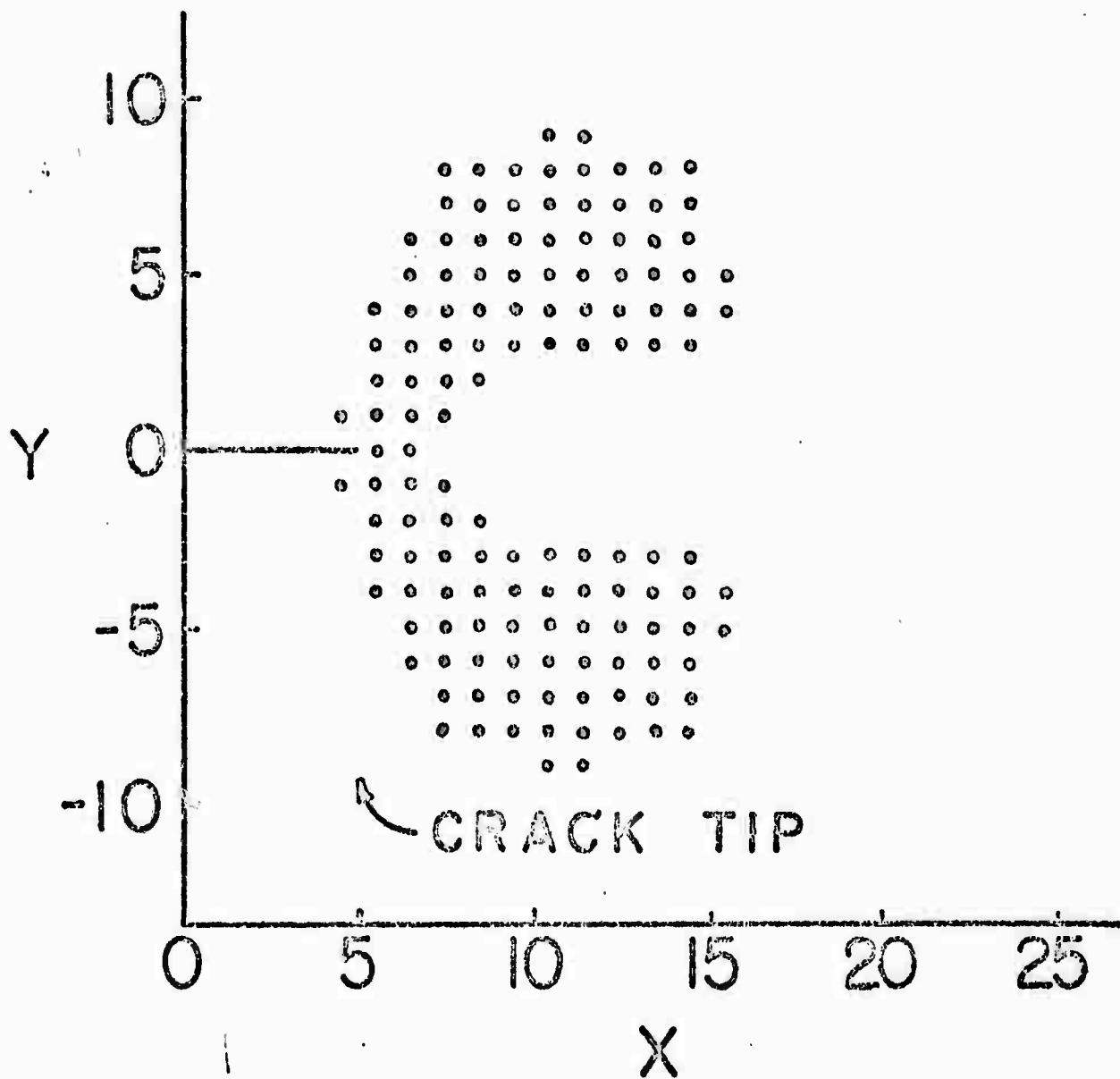


FIG. 13
- 55 -